

This manuscript is a preprint and has been submitted for publication in *Applied Spectroscopy*. Take into consideration that the manuscript has yet to be formally accepted for publication and may have slightly different content between the preprint and accepted version. The final version of this manuscript will be available via the publication DOI link. Please feel free to contact any of the authors.

1 ***In-situ* quantification of carbonate species concentrations, pH and pCO₂ in calcite fluid**
2 **inclusions using confocal Raman spectroscopy.**

3 Michael Naylor Hudgins ^{a,b*}, Todd K. Knobbe ^a, Julia Hubbard ^a, Andrew Steele ^c, Justin G.
4 Park^{a,b}, and Morgan F. Schaller ^{a,b*}

5 ^a *Department of Earth and Environmental Sciences, Rensselaer Polytechnic Institute, Jonsson*
6 *Rowland Science Center, Troy, NY, USA*

7 ^b *Rensselaer Astrobiology Research and Education Center, Rensselaer Polytechnic Institute,*
8 *Jonsson Rowland Science Center, Troy, NY, USA*

9 ^c *Earth and Planets Laboratory, Carnegie Institution for Science, Washington, DC, USA*

10 *Corresponding Author: schall@rpi.edu

11 *Co-corresponding Author: hudgim@rpi.edu

12 **Abstract**

13 Carbonate minerals are globally distributed on the modern and ancient Earth and are abundant in
14 terrestrial and marine depositional environments. Fluid inclusions hosted by calcite retain primary
15 signatures of the source fluid geochemistry at the time of mineral formation (i.e., pCO₂) and can
16 be used to reconstruct paleoenvironments. Confocal laser Raman spectroscopy provides a quick,
17 non-destructive approach to measuring the constituents of fluid inclusions in carbonates and is a
18 reliable method for determining composition in both the aqueous and gas phases in fluid
19 inclusions. Here, we demonstrate a method for making accurate quantifications of carbonate
20 concentrations and pH from fluid inclusions using confocal Raman spectroscopy. Instrument
21 calibrations for carbonate (CO₃²⁻) and bicarbonate (HCO₃⁻) concentrations and pH were performed
22 using stock solutions. The host mineral does not affect the carbonate species. Accurate
23 quantification of carbonate solution concentrations and pH can be used to estimate the pCO₂ of a
24 solution when measuring fluid inclusions with Raman spectroscopy.

25

26 **Introduction**

27 Fluid inclusions provide a wealth of information pertaining to a mineral's environment at
28 the time of formation^{1,2}. The ability to quantify the constituents within fluid inclusions provides

29 information on geochemical parameters such as; initial temperature and pressure conditions,
30 salinity, pH, and solution and gas composition of any included gas phases³⁻⁹. These geochemical
31 indicators can be estimated by using Raman spectroscopy, a non-destructive method, that can be
32 applied to the *in-situ* study of micron-scale fluid inclusions^{6,10-14}.

33 Calcium carbonate minerals are common and abundant in a variety of environmental
34 settings on Earth, ranging from metamorphic carbonates forming in subduction zones¹⁴ to low
35 temperature authigenic marine sediments¹⁵ and surficial deposits (pedogenic or speleothems)^{16,17}.
36 Many of these types of carbonates can contain fluid inclusions, in metamorphic carbonates they
37 have been used to track carbon transport in Earth's interior¹⁴ and in low-temperature carbonates
38 fluid inclusions have been used to measure paleoenvironmental proxies in both the terrestrial and
39 marine realms¹⁵⁻¹⁸. Many studies have focused on carbon and oxygen isotopic compositions of
40 either the mineral matrix or fluid within inclusions¹⁶⁻¹⁹, but relatively fewer studies have
41 investigated the gas concentration or aqueous composition of fluid inclusions in non-diagenetic
42 carbonate minerals^{15,20,21}.

43 A fundamental problem in paleoclimatology is the lack of accurate atmospheric pCO₂
44 estimates prior to the ice core record²². The proxy methods that have been deployed (e.g., the
45 δ¹³C of pedogenic carbonates, leaf stomatal indices, and boron isotopes^{16,23-25}) show similar
46 trends but disagree in absolute value²³⁻²⁹. However, dissolved gases and solutes in the aqueous
47 phase of carbonate mineral fluid inclusions can provide valuable insight into the geochemical
48 conditions of the mineral's formation environment, which can be related back to absolute
49 atmospheric concentrations at the time of precipitation^{1-4,7,30}. Unfortunately, these analyses
50 require the destruction of fluid inclusions during bulk analyses of the released gases and require
51 large sample sizes to enable accurate measurement³¹⁻³³. In contrast, Raman spectroscopy is a

52 non-destructive method that can provide rapid analyses of liquid and gas phase compositions
53 within individual fluid inclusions^{5,34}. This method enables each of the components of the
54 carbonate system (e.g., $[\text{CO}_3^{2-}]$, $[\text{HCO}_3^-]$, pH, and pCO_2) to be quantified discretely *in-situ*
55 without disturbing the host mineral matrix. However, before quantification of any molecules
56 measured directly within natural fluid inclusion samples, the mineral system's Raman spectrum
57 and the host mineral's effects on solute quantification need to be evaluated.

58 Identification and quantification of the carbonate species (e.g., CO_3^{2-} , HCO_3^-)
59 concentration provides information on solution pH and pCO_2 of the system that the mineral
60 precipitated in³⁵. In moderately alkaline systems, HCO_3^- is the dominant carbon species in
61 solution, and the Raman signal of HCO_3^- has been observed in alkaline solutions in quartz hosted
62 fluid inclusions^{14,36,37}. However, these studies only recorded the presence of HCO_3^- and did not
63 attempt to quantify the concentration. Although a weak Raman scatterer, detailed studies have
64 shown that HCO_3^- is amenable to quantification over a range of concentrations using Raman
65 spectroscopy³⁸⁻⁴⁰. However, these studies did not address the applicability of Raman
66 spectroscopy to quantifying HCO_3^- concentrations in natural samples.

67 In this study, we present a method for the accurate measurement of $[\text{CO}_3^{2-}]$ and $[\text{HCO}_3^-]$
68 in fluid inclusions via Raman spectroscopy and use these measurements to estimate the pCO_2
69 with which the inclusion fluid had equilibrated. We construct calibration curves for CO_3^{2-} and
70 HCO_3^- using Na_2CO_3 and NaHCO_3 solutions via two different methods (with and without the
71 addition of a calcite cover slip to examine the effects of the host mineral)⁴¹, with the ultimate
72 goal of applying these calibrations to natural carbonate samples. We then evaluate the accuracy
73 of each method to determine the most suitable approach for determining the concentration of
74 CO_3^{2-} and HCO_3^- in natural fluid inclusions. We also investigate the effect of increasing solution

75 salinity on the quantification of solutes in fluid inclusions. These studies reveal that $[\text{CO}_3^{2-}]$,
76 $[\text{HCO}_3^-]$, and the pH of alkaline solutions can be determined using the main Raman bands for
77 CO_3^{2-} and HCO_3^- . The approaches and methods developed in this paper can be applied to a range
78 of fluid inclusions at 1 atm. The specific effects of temperature and pressure broadening on
79 Raman peak parameters of $[\text{CO}_3^{2-}]$, $[\text{HCO}_3^-]$ are not addressed in this study and has been
80 investigated elsewhere^{42,43}.

81 **Methods**

82 *Calibration Solutions*

83 Prior Raman calibration studies for CO_3^{2-} and HCO_3^- in solution have been made at
84 concentrations spanning from dilute solutions to near saturation ($[\text{HCO}_3^-]$: 1.57-0.0521 molar;
85 $[\text{CO}_3^{2-}]$: 1.55-0.000019 molar)^{38,44,45}. Here, we focus on calibrating the Raman response to CO_3^{2-}
86 and HCO_3^- concentrations in dilute carbonate solutions that are closer to those observed in
87 natural systems (Table 1). We prepared solutions of Na_2CO_3 and NaHCO_3 over a range of $[\text{CO}_3^{2-}]$
88 $[\text{HCO}_3^-]$, and pH that represent observed concentrations of natural systems^{35,46-52} (Table 1 and
89 2). Natural fluid inclusions in carbonates forming at the surface and in seawater have a range of
90 salinities³. Therefore, we also constructed calibrations over a range of NaCl salinities (1-5 wt%)
91 to more closely resemble natural systems and to investigate salinity effects on the Raman peak
92 response of carbonate species and pH quantification. We consider NaCl calibrations necessary
93 because previous studies have demonstrated that increasing salinity alters the dissociation and
94 solubility constants (K_{CO_2} , K_1 , and K_2) and skews the OH^- stretch of H_2O ^{8,53,54}, thus potentially
95 leading to an inaccurate estimation carbonate species concentrations where freshwater calibration
96 curves are applied to saline inclusions.

97 A portion of solutions were equilibrated to the atmosphere and the remainder were
98 prepared as a close system, to encompass a full range of relevant carbonate species
99 concentrations. Desired weights of NaHCO₃, Na₂CO₃, and NaCl were placed in 50 mL centrifuge
100 tubes and continuously mixed with 50 mL of Millipore water (18 Ω) until fully dissolved. Open
101 system solutions were mixed until equilibrium was reached. To obtain a pH <8, 1.2 molar HCl
102 (10% HCl by volume) was added to a 0.25 molar of NaHCO₃ solutions. Once the acid was
103 added, the solution was mixed until a stable pH was reached. Solution temperature and pH were
104 measured with a Thermo Scientific Orion 2-star pH meter before measurement by Raman.

105 To calculate the amount of HCO₃⁻ and CO₃²⁻ in the closed system solutions at the time of
106 measurement, the initial amount of HCO₃⁻ and CO₃²⁻ mixed in the solution was assumed to be
107 equal to the total dissolved inorganic carbon (TDIC). Aqueous speciation of the closed carbonate
108 system were calculated based on measured temperature and pH using the following equations⁵⁵
109 (Eq. 1 and 2):

$$110 \quad [\text{HCO}_3^-] = C_T \frac{K_1[\text{H}^+]}{[\text{H}^+]^2 + K_1[\text{H}^+] + K_1K_2}$$

111 Eq. 1

$$112 \quad [\text{CO}_3^{2-}] = C_T \frac{K_1K_2}{[\text{H}^+]^2 + K_1[\text{H}^+] + K_1K_2}$$

113 Eq. 2

114 Where [HCO₃⁻] is molar HCO₃⁻; [CO₃²⁻] is molar CO₃²⁻; C_T is molar TDIC (the initial
115 amount of HCO₃⁻ and CO₃²⁻ put into solution as a NaHCO₃ and Na₂CO₃ salt); K₁ and K₂ are
116 temperature-dependent equilibrium constants that account for the dissociation of H₂CO₃ and
117 HCO₃⁻, respectively; and [H⁺] is molar hydrogen ions.

118 For solutions prepared as an open system, HCO_3^- and CO_3^{2-} concentrations were
119 calculated based on the open system equations⁵⁶:

$$120 \quad [\text{HCO}_3^-] = \frac{K_1 K_{\text{CO}_2} p\text{CO}_2}{[\text{H}^+]}$$

121 Eq. 3

$$122 \quad [\text{CO}_3^{2-}] = \frac{K_1 K_2 K_{\text{CO}_2} p\text{CO}_2}{[\text{H}^+]^2}$$

123 Eq. 4

124 K_{CO_2} (i.e., Henry's constant) is the temperature-dependent equilibrium constant that
125 accounts for the aqueous solubility of CO_2 . When estimating carbonate species concentrations
126 for the calibrations, the equilibrium constants were adjusted to the measured temperature values
127 using the calculations of Drever (1997)⁵⁶.

128 We used the closed system calculations to estimate $p\text{CO}_2$ in natural fluid inclusions,
129 because the trapped solute acts as a closed system post-entrapment and the components of the
130 fluid (alkalinity, TDIC, pH, and $p\text{CO}_2$) are fixed. However, the fluid inclusion would represent
131 the environment pre-entrapment as the solute was equilibrated with the atmosphere, assuming
132 the mineral formed at the Earth's surface. Therefore, fluid inclusions behave as a closed system
133 and estimations of $p\text{CO}_2$ should use such equations.

134 Closed system estimations of $p\text{CO}_2$ require information on $[\text{CO}_3^{2-}]$, $[\text{HCO}_3^-]$, $[\text{CO}_2 \text{ aq}]$,
135 and pH. Our calibrations can quantify $[\text{CO}_3^{2-}]$, $[\text{HCO}_3^-]$, and pH, but estimating $[\text{CO}_2 \text{ aq}]$ must be
136 calculated because its concentration is low in the natural range chosen in this study⁵⁵ (Table 2).
137 To estimate $[\text{CO}_2 \text{ aq}]$ we use the following equation:

$$138 \quad [\text{CO}_2 \text{ aq}] = [\text{H}^+]^2 \frac{[\text{CO}_3^{2-}]}{K_1 K_2}$$

139 Eq. 5

140 Which allows for pCO₂ to be estimated from the calculated [CO_{2 aq}]:

141
$$pCO_2 = \frac{[CO_{2 aq}]}{K_{co2}}$$

142 Eq. 6

143 To ensure that the range of [CO₃²⁻] and [HCO₃⁻] captures a large range of pCO₂ values,
144 theoretical estimations were performed using the carbonate closed system equations (Eq. 1, 2,
145 and 5) and solved for pCO₂ (Fig. 1). These calculations show that the ratio between [CO₃²⁻] and
146 [HCO₃⁻], and pH can be used to estimate a wide range of pCO₂ (-4 to 0) values (Fig. 1). The
147 [CO₃²⁻], [HCO₃⁻], and pH of the Na₂CO₃ and NaHCO₃ solutions were input into the carbonate
148 closed system equations to calculate the range of potential pCO₂ values. Figure 1 shows that the
149 concentrations we selected for our solutions can be used to estimate a wide range (-4 to 0) of
150 pCO₂.

151

152 *Evaluating the Effect of the Carbonate Host Mineral*

153 To evaluate whether the host mineral's birefringence affects the calibration curves of
154 solute concentrations and pH in a natural carbonate sample, a cover slip was made from optical
155 grade calcite to simulate the measurement of a calcite-hosted fluid inclusion. Previous research
156 has demonstrated that the host mineral does not affect determination of salt concentrations in
157 calcite when using a confocal Raman Spectrometer^{8,41}. These authors suggest minimizing the
158 effect of the host mineral in Raman spectroscopy micro-fluid inclusion studies by placing the
159 sample at its extinction position. To test this, a piece of optical grade calcite that has the c-axis
160 parallel to surface and free of visible inclusions and defects was used in a subset of

161 measurements to ensure the host mineral does not affect solute quantification. The cover slip was
162 ground to a thickness of ~100 microns and doubly polished to a colloidal silica grade.

163 A comparison of the standard NaHCO_3 and Na_2CO_3 solutions measured by Raman both
164 with and without the addition of a calcite cover slip was performed for each concentration to
165 measure the effect of the host mineral on solute quantification (Fig. 2). To ensure that the desired
166 focal plane was in the solution, before each measurement, the laser was first focused on the
167 surface of the cover slip and then focused down to the underside of the cover slip, and finally
168 focused 100 microns below and into the solution. For solutions without the calcite cover slip, the
169 laser was focused 100 microns below the surface of the solution.

170

171 *Raman Measurement and quantification of CO_3^{2-} and HCO_3^-*

172 Shortly after a solution was mixed and the open system solutions reached equilibrium, 5
173 microliters of solution were placed in a glass concavity slide and analyzed using a WiTec
174 alpha300 R confocal Raman spectrometer utilizing a 532 nm green laser at the Carnegie Institute
175 of Science, Earth and Planets Laboratory⁵⁷. Laser power at the source was 14 mW during each
176 analysis. Measurements were made using a Zeiss 50x objective, a 50 μm aperture, and a 1 cm^{-1}
177 spectral resolution using a Witec UHTS spectrometer system with a 600 grating and an Andor
178 DV400 camera cooled to -59 °C. Additional measurements were made on a Bruker SENTERRA
179 Raman spectrometer at Rensselaer Polytechnic Institute, Department of Earth and Environmental
180 Science. Measurements were integrated for 30 seconds with 3 accumulations and alternated
181 between the solution and the solution with calcite cover slip to minimize any evolution in the
182 solution composition over the course of the analyses. Each component (H_2O , HCO_3^- , and CO_3^{2-}
183 solution with and without the calcite cover slip, and the calcite cover slip alone) used in this

184 study can be broken down into their individual Raman spectra (i.e., H₂O, CaCO₃, etc. measured
185 independently), and when constructed together, form a spectra that simulates a fluid inclusion
186 (Fig.2).

187 The HCO₃⁻ anion has a weak Raman scatter, but in alkaline solutions, HCO₃⁻ is the
188 dominant anion of the carbonate system and has 9 normal, partially polarized Raman modes
189 ^{5,40,58}. The two broad, weak peaks at 634 cm⁻¹ and 673 cm⁻¹ with the latter representing δCO₂.
190 The broad mode at 634 cm⁻¹ can be deconvoluted into three sub-bands at 630 cm⁻¹, 634 cm⁻¹, and
191 640 cm⁻¹ to represent γCO-H and δHOC. HCO₃⁻ modes are prevalent at 843 cm⁻¹ (γCO₃), 1017
192 cm⁻¹ (νC-OH), 1312 cm⁻¹ (δCO-H), 1360 cm⁻¹ (ν_sCO₂), 1630 cm⁻¹ (ν_{as}CO₂), and 2600 cm⁻¹ (νCO-
193 H)⁴⁰. The Raman bands of CO₃²⁻ have 6 active Raman modes^{5,38}, where weak peaks occur at 684
194 cm⁻¹ (ν₄, in-plane deformation), 885 cm⁻¹ (ν₂, out-of-plane deformation), 1385 cm⁻¹ (ν₃,
195 antisymmetric stretch C-O), 1435 cm⁻¹, and 1764 cm⁻¹⁴⁰. However, to avoid issues with peak
196 interferences, low intensity signals, and/or mineral fluorescence, the main vibrational mode of
197 HCO₃⁻ at 1017 cm⁻¹ and CO₃²⁻ at 1066 cm⁻¹ was used to quantify the amount of [HCO₃⁻] and
198 [CO₃²⁻] in solutions as these are the strongest peaks^{5,40}. Calibration solution data was exported in
199 OriginLab (OriginLab Corp., Northampton, MA, USA) where the spectra was background
200 subtracted and the main HCO₃⁻ and CO₃²⁻ bands were integrated for their cumulative area (A_{HCO₃⁻}
201 ₃₋ and A_{CO₃²⁻}). The area of the HCO₃⁻ and CO₃²⁻ bands were ratioed (A_{CO₃²⁻}/A_{HCO₃⁻}) as this
202 parameter is reliable in estimating pH, as well as [CO₃²⁻], and [HCO₃⁻] as the concentrations are
203 pH dependent (Fig. 1). The ratioed area of the bands, the measured pH, and the calculated
204 [HCO₃⁻] and [CO₃²⁻] of calibration solutions are used to build calibration curves which allows us
205 to estimate [CO₃²⁻], [HCO₃⁻], and pH of an unknown sample^{38,59}.

206 *Optical Calcite Fluid Inclusion*

207 An Icelandic Spar calcite sample of an unknown origin was used to evaluate the
208 applicability of our calibration's curves to natural carbonate samples. The Icelandic Spar calcite
209 was chosen as a test sample, as it contained an abundance of primary and secondary fluid
210 inclusions spanning a large size range. An inclusion-free portion of the same mineral was used to
211 make the calcite cover slip and provides the best matrix matched sample to test the calibration
212 curves. The fluid inclusions in the Icelandic Spar calcite are predominantly of two phases, vapor
213 and liquid. For demonstration of the success of the calibration technique, a large inclusion that is
214 ~150 μm across and ~150 μm below the sample surface was analyzed. Measurements were
215 focused on a large ~150 μm fluid inclusion because the area of the phases (aqueous or vapor) of
216 interest were larger than the laser spot size (~1 μm or less). Fluorescence from the host calcite
217 makes it increasingly difficult to analyze small inclusions, especially as parameters such as
218 integration time and accumulations are increased. If carbonate species concentrations and pH of
219 the solution are quantified, then the pCO_2 can be determined in a fluid inclusion using equation
220 six⁵⁵. The spectra of the Icelandic Spar calcite were processed and deconvoluted as the
221 calibration solution, as described in the previous section.

222

223 **Results and Discussion**

224 *Calibration Curves*

225 Aqueous bicarbonate and carbonate calibration curves were made for a range of solution
226 to calibrate the Raman spectrometer to quantify carbonate species concentrations and pH and to
227 investigate the effects of the host mineral and salinity on carbonate species and pH
228 quantification.

229 Area ratio calibrations for standard solutions (without NaCl) with and without the calcite
230 cover slip are similar (Fig. 3 and Table 3; consult this table for equations). Quantification of
231 $[\text{CO}_3^{2-}]$, $[\text{HCO}_3^-]$, and pH using $A_{\text{CO}_3^{2-}}/A_{\text{HCO}_3^-}$ show a power, linear, and exponential
232 relationship, respectively, with and without the calcite cover slip (Fig. 3). NaCl wt% calibration
233 curves display a spreading pattern for $[\text{CO}_3^{2-}]$ and pH estimations with increasing salinity,
234 whereas $[\text{HCO}_3^-]$ have similar slopes and intercepts (Fig. 4 and Table 4; consult this table for
235 equations). Quantification of $[\text{CO}_3^{2-}]$, $[\text{HCO}_3^-]$, and pH using $A_{\text{CO}_3^{2-}}/A_{\text{HCO}_3^-}$ with increasing
236 salinity shows a power, linear, and exponential relationship, respectively.

237 *Characterization of the Raman spectra*

238 The solutions with the calcite cover slip have a peak at 1088 cm^{-1} that may interfere with
239 CO_3^{2-} in solution and can pose a potential problem in accurately quantifying carbonate species at
240 low concentrations in fluid inclusions, as discussed in Dubessy et al. (1992)¹². However, the
241 confocal Raman spectrometer also detects a low CaCO_3 peak at 1088 cm^{-1} that does not interfere
242 with the CO_3^{2-} signal (Fig. 2). With this, the calcite cover slip has little to no effect on estimating
243 $[\text{CO}_3^{2-}]$, $[\text{HCO}_3^-]$, and pH of the system when using area ratio between the carbonate species. At
244 lower concentrations, HCO_3^- and CO_3^{2-} becomes harder to distinguish from the background (pH
245 $= < 7$) and perhaps an additional extrapolation scheme may be needed.

246 Caumon et al. (2015)⁴¹ demonstrated that if the crystal symmetry and optical properties
247 are not accounted for then quantification errors can occur. However, this is not a concern in our
248 analyses because we employ a confocal Raman spectrometer which bypasses the calcite cover
249 slip as it is above the focal point and does not contribute to the analysis^{34,60}. Given this, there is
250 no substantial difference expected, and accordingly little effect is observed on the calibration
251 curves between non- and calcite cover slip analyses (Fig. 3). The confidence intervals indicate no

252 major differences between non-calcite cover slip and calcite cover slip as they overlap one
253 another (Table 3).

254 The effects of salinity on the calibrations at low $[\text{CO}_3^{2-}]$ and pH is likely negligible
255 ($[\text{CO}_3^{2-}] < 0.01$ molar and ~ 9.5 pH) (Fig. 4). However, accounting for salinity in estimating
256 $[\text{HCO}_3^-]$ is likely minor at all concentrations as the slope of the calibrations for different
257 salinities overlap within their respective confidence intervals (Fig. 4 and Table 4). Therefore, it
258 may be unnecessary to account for the effects of salinity for a solution at low concentrations
259 (e.g., seawater) and pH in natural fluid inclusions. Although, at higher $[\text{CO}_3^{2-}]$ and pH, salinity
260 should be considered by using the OH⁻ Raman stretch to quantify the concentration of NaCl^{6,8}.
261 Their methods to determine NaCl concentration can be applied to natural fluid inclusions to
262 allow for accurate $[\text{CO}_3^{2-}]$, $[\text{HCO}_3^-]$, and pH estimates using our calibrations. Overall, the
263 relationships observed are a promising approach towards accurately quantifying carbonate
264 species and pH to estimate $p\text{CO}_2$ in natural samples.

265 *Measurement of fluid inclusion in Calcite*

266 The results of measurements of the aqueous and gaseous phases of a ~ 150 microns fluid
267 inclusion in the Icelandic Spar calcite are shown in Figure 5. The inclusion formed in an area of
268 the crystal that showed no signs of fracture healing or continual mineral growth along a growth
269 plane⁶¹. Because the origin, internal pressure, density, and temperature of formation of the fluid
270 inclusion is unknown, this section and the measurements described within are presented as a
271 demonstrative proof of concept. We chose this sample for its ample size. Given this, the density
272 of the gaseous phase CO_2 can be determined by using the Fermi diad peak difference ($\nu_1 - 2\nu_2$) of
273 CO_2 ^{62,63}. It is worth noting that although fluid inclusion homogenization experiments can be used
274 to determine temperature of formation, it is beyond the scope of this study.

275 In the aqueous phase spectra, the distinctive peaks of the calcite host mineral can be
276 observed as well as a HCO_3^- and CO_3^{2-} peak at 1017 cm^{-1} and 1066 cm^{-1} , respectively (Fig. 5).
277 The OH^- stretch is present between $2750\text{-}3700\text{ cm}^{-1}$. The salinity in the fluid inclusion was
278 estimated to be 19.9 wt% using the equation of Wang et al. (2013), assuming that NaCl only is
279 present in solution⁶⁴. The area between the HCO_3^- and CO_3^{2-} peaks were calculated, ratioed, and
280 applied to the calibration curves without the calcite cover slip. pH was estimated to be $9.46 \pm$
281 0.31 , and $[\text{HCO}_3^-]$ and $[\text{CO}_3^{2-}]$ were determined to be 0.04 ± 0.02 and 0.05 ± 0.08 molar,
282 respectively (Table 5). The dissociation and solubility constants were adjusted to the measured
283 salinity value using the calculations of Millero (2006)⁵³ and Onda et al. (1970)⁵⁴. 20C° was
284 assumed for the solubility and dissociation constants to calculate pCO_2 because the temperature
285 at the time of formation is unknown. With carbonate concentrations and solution pH estimated,
286 $\text{pCO}_{2(\text{g})}$ was calculated to be -3.62 ± 0.19 (240 ± 132 ppm).

287 In the gaseous phase spectra, the CO_2 Fermi diad is present at 1287 cm^{-1} and 1389 cm^{-1} ,
288 hydrogen sulfide and methane are also present at 2611 cm^{-1} and 2917 cm^{-1} , respectively⁵ (Fig. 5).
289 The density of CO_2 is essentially zero as the fermi diad technique can be utilized as low as 0.1
290 g/cm^3 ^{62,63}. However, the density of present-day atmospheric CO_2 is 0.0019 g/cm^3 , potentially
291 suggesting that the fluid inclusion formed in an atmosphere between <0.0019 and $<0.1\text{ g/cm}^3$ of
292 CO_2 . In addition, the lack of major atmospheric gases (e.g., O_2 and N_2), the presence of H_2S and
293 CH_4 suggest that the fluid inclusion precipitated in a reducing environment.

294

295 *Calibration Limitations*

296 Quantification of $[\text{CO}_3^{2-}]$, $[\text{HCO}_3^-]$, and pH can provide information about the pCO_2 of
297 formation of a carbonate fluid inclusion, and there is no observed effect from the host mineral on

298 estimating pH and carbonate species when using a confocal instrument (Fig. 3)^{8,41}. However,
299 there are limitations using this method, including: (1) the Raman spectrometer was calibrated at
300 low temperatures and pressures (1 atm), where it is likely the calibrations will deviate at higher
301 temperatures and pressures as the solubilities and the dissociation constants of the carbonate
302 species change^{65,66}. (2) The calibrated Raman spectrometer does not encompass the low pH
303 range present in modern^{48,52} and ancient systems⁴⁶ (e.g., acidic springs and soils). (3)
304 Determining the alkalinity of fluid inclusions may be impossible with current technology as
305 titrating them would lead to fluid contamination. However, it is reasonable to assume that the
306 alkalinity would be controlled by TDIC, as it is in the modern oceans⁶⁷. (4) Salts (e.g., MgCl₂,
307 CaCl₂, and KCl) are likely to be present in natural carbonate fluid inclusions that will skew the
308 water peaks^{8,64} and may affect accurate determination of pH and species concentrations. (5)
309 Analyses of fluid inclusions are based on small amounts of solution, and this limits the
310 determination of carbonate species concentrations and pH, as a relationship exists between the
311 intensity and the number of molecules present in the sample⁶⁸. For example, if there is a limited
312 amount of water in a carbonate fluid inclusion, a lower intensity water peak will be observed,
313 and as a consequence of this, the HCO₃⁻ and CO₃²⁻ peaks may not be detectable in these
314 inclusions. However, larger carbonate fluid inclusions are promising as more solution is present
315 and may be able to detect HCO₃⁻ and CO₃²⁻ (Fig. 5).

316 *Other Applications*

317 The different proxies to estimate pCO₂ in deep time do not agree with one another^{16,23–25}.
318 For example, data from δ¹³C of paleosol carbonates and stomatal indices of fossil plants from the
319 end-Triassic extinction show a corroborating pCO₂ trend, but the absolute pCO₂ values do not
320 agree^{26–28}. One reason is the soil productivity parameter (S(z)) within the soil diffusion model²⁵.

321 This parameter is the concentration of CO_2 in the soil derived from the respiration of organic
322 matter and CO_2 in the atmosphere. CO_2 estimations within a soil is largely unknown and
323 unconstrained because this parameter will fluctuate depending on soil profile depth and soil
324 type¹⁶. However, the calibration presented in this study is a potential method that can constrain
325 the $S(z)$ and estimate pCO_2 within a soil column.

326 **Conclusion**

327 We demonstrate the calibration of a confocal Raman spectrometer over a range of $[\text{CO}_3^{2-}]$,
328 $[\text{HCO}_3^-]$, and pH, representative of natural waters. These calibrations allow for the
329 quantification of carbonate species concentrations and pH in fluid inclusion at low-temperatures
330 and pressures. Calibrations can be used to calculate $[\text{CO}_3^{2-}]$, $[\text{HCO}_3^-]$, and pH, which ultimately
331 allows pCO_2 to be determined in mineral fluid inclusions, assuming the mineral formed at the
332 Earth's surface and equilibrated with its environment. The host mineral's crystal optics have
333 little to no effect on determining the $[\text{CO}_3^{2-}]$, $[\text{HCO}_3^-]$, and pH if the Raman spectrometer is
334 confocal. Negligible effects of salinity occur at low $[\text{CO}_3^{2-}]$ and pH, and all $[\text{HCO}_3^-]$.
335 Homogenization temperature experiments should be conducted in conjunction with confocal
336 Raman experiments to determine accurate pCO_2 estimations in natural fluid inclusions.

337 **Acknowledgements**

338 This research was supported by NASA Earth First Origins grant A129942527. We would
339 like to thank Oliver Wolfe, Samantha Pyror, Nikos Sitaras, Sebastian Barkett, Mikayla Berman,
340 Kristin Johnson-Finn, Jacob Shelley, Frank Spear, and Kristen Chiamo for enlightening
341 discussions, edits, and feedback that greatly improved this manuscript. The authors thank the
342 anonymous reviewers for their valuable feedback, and suggestions that greatly improved the
343 quality of the manuscript.

344 **References**

- 345 1. R.H. Goldstein. “Clues from Fluid Inclusions”. *Science*. American Association for the
346 Advancement of Science, 2001. 294(5544): 1009–1011. 10.1126/science.1066322.
- 347 2. E. Roedder. “Introduction to Fluid Inclusions”. Mineralogical Society of America. 1984. 12:
348 1–10.
- 349 3. R.J. Bodnar. Chapter 4. Introduction to Aqueous-Electrolyte Fluid Inclusions. Mineral.
350 Assoc. Canada, 2003.
- 351 4. L.W. Diamond. Chapter 3. Systematics of H₂O Inclusions. Mineral. Assoc. Canada, 2003.
- 352 5. M.L. Frezzotti, F. Tecce, A. Casagli. “Raman spectroscopy for fluid inclusion analysis”.
353 *Journal of Geochemical Exploration*. 2012. 112: 1–20. 10.1016/j.gexplo.2011.09.009.
- 354 6. T.P. Mernagh, A.R. Wilde. “The use of the laser Raman microprobe for the determination of
355 salinity in fluid inclusions”. *Geochimica et Cosmochimica Acta*. 1989. 53(4): 765–771.
356 10.1016/0016-7037(89)90022-7.
- 357 7. T.K. Lowenstein, M.N. Timofeeff, S.T. Brennan, L.A. Hardie, R.V. Demicco. “Oscillations
358 in Phanerozoic Seawater Chemistry: Evidence from Fluid Inclusions”. *Science*. American
359 Association for the Advancement of Science, 2001. 294(5544): 1086–1088.
360 10.1126/science.1064280.
- 361 8. Q. Sun, L. Zhao, N. Li, J. Liu. “Raman spectroscopic study for the determination of Cl-
362 concentration (molarity scale) in aqueous solutions: Application to fluid inclusions”.
363 *Chemical Geology*. 2010. 272(1–4): 55–61. 10.1016/j.chemgeo.2010.02.004.
- 364 9. T. Azbej, M.J. Severs, B.G. Rusk, R.J. Bodnar. “In situ quantitative analysis of individual
365 H₂O–CO₂ fluid inclusions by laser Raman spectroscopy”. *Chemical Geology*. 2007. 237(3–
366 4): 255–263. 10.1016/j.chemgeo.2006.06.025.
- 367 10. Brigitte. Wopenka, J.Dill. Pasteris. “Raman intensities and detection limits of geochemically
368 relevant gas mixtures for a laser Raman microprobe”. *Anal. Chem*. 1987. 59(17): 2165–2170.
369 10.1021/ac00144a034.
- 370 11. J. Dubessy, B. Poty, C. Ramboz. “Advances in C-O-H-N-S fluid geochemistry based on
371 micro-Raman spectrometric analysis of fluid inclusions”. *European Journal of Mineralogy*.
372 1989. 1(4): 517–534.
- 373 12. J. Dubessy, M.-C. Boiron, A. Moissette, C. Monnin, N. Sretenskaya. “Determination of
374 water, hydrates and pH in fluid inclusions by micro-Raman spectrometry”. *European Journal*
375 *of Mineralogy*. 1992. 4: 885–894. 10.1127/ejm/4/5/0885.
- 376 13. E.A.J. Burke. “Raman microspectrometry of fluid inclusions”. *Lithos*. 2001. 55(1): 139–158.
377 10.1016/S0024-4937(00)00043-8.
- 378 14. M.L. Frezzotti, J. Selverstone, Z.D. Sharp, R. Compagnoni. “Carbonate dissolution during
379 subduction revealed by diamond-bearing rocks from the Alps”. *Nature Geosci*. Nature
380 Publishing Group, 2011. 4(10): 703–706. 10.1038/ngeo1246.
- 381 15. U. Brand, N. Blamey, C. Garbelli, E. Griesshaber, R. Posenato, L. Angiolini, et al. “Methane
382 Hydrate: Killer cause of Earth’s greatest mass extinction”. *Palaeoworld*. 2016. 25(4): 496–
383 507. 10.1016/j.palwor.2016.06.002.

- 384 16. T.E. Cerling. “Stable Carbon Isotopes in Palaeosol Carbonates”. In: M. Thiry, R. Simon-
385 Coinçon, editors. *Palaeoweathering, Palaeosurfaces and Related Continental Deposits*.
386 Blackwell Publishing Ltd., Oxford, UK, 2009. Pp. 43–60. 10.1002/9781444304190.ch2.
- 387 17. M.L. Griffiths, R.N. Drysdale, H.B. Vonhof, M.K. Gagan, J. Zhao, L.K. Ayliffe, et al.
388 “Younger Dryas–Holocene temperature and rainfall history of southern Indonesia from $\delta^{18}\text{O}$
389 in speleothem calcite and fluid inclusions”. *Earth and Planetary Science Letters*. 2010.
390 295(1): 30–36. 10.1016/j.epsl.2010.03.018.
- 391 18. N. Tabor, T. Myers. “Paleosols as Indicators of Paleoenvironment and Paleoclimate”. *Annual*
392 *Review of Earth and Planetary Sciences*. 2014. 43: 150317182938004. 10.1146/annurev-
393 earth-060614-105355.
- 394 19. H.P. Schwarcz, R.S. Harmon, P. Thompson, D.C. Ford. “Stable isotope studies of fluid
395 inclusions in speleothems and their paleoclimatic significance”. *Geochimica et*
396 *Cosmochimica Acta*. 1976. 40(6): 657–665. 10.1016/0016-7037(76)90111-3.
- 397 20. K. Azmy, N.J.F. Blamey. “Source of diagenetic fluids from fluid-inclusion gas ratios”.
398 *Chemical Geology*. 2013. 347: 246–254. 10.1016/j.chemgeo.2013.04.011.
- 399 21. N. Blamey, N.M.I. of Mining, P. Boston, L. Rosales-Lagarde, N.M.I. of Mining, N.S.
400 College. “High-resolution signatures of oxygenation and microbiological activity in
401 speleothem fluid inclusions”. *International Journal of Speleology*. 2016. 45(3): 231–241.
- 402 22. D. Lüthi, M. Le Floch, B. Bereiter, T. Blunier, J.-M. Barnola, U. Siegenthaler, et al. “High-
403 resolution carbon dioxide concentration record 650,000–800,000 years before present”.
404 *Nature*. 2008. 453(7193): 379–382. 10.1038/nature06949.
- 405 23. D.L. Royer, K.M. Moynihan, M.L. McKee, L. Londoño, P.J. Franks. “Sensitivity of a leaf
406 gas-exchange model for estimating paleoatmospheric CO_2 concentration”. *Climate of the*
407 *Past*. Copernicus GmbH, 2019. 15(2): 795–809. 10.5194/cp-15-795-2019.
- 408 24. S.M. Eggins, L.L. Haynes, K.A. Allen, K.D. Holland, K. Lorbacher, B. Hönisch. *Boron*
409 *Proxies in Paleoceanography and Paleoclimatology*. 1st edition. Wiley-Blackwell, Hoboken,
410 NJ, 2019.
- 411 25. D.O. Breecker. “Quantifying and understanding the uncertainty of atmospheric CO_2
412 concentrations determined from calcic paleosols”. *Geochemistry, Geophysics, Geosystems*.
413 2013. 14(8): 3210–3220. 10.1002/ggge.20189.
- 414 26. M.F. Schaller, J.D. Wright, D.V. Kent. “Atmospheric Pco_2 Perturbations Associated with the
415 Central Atlantic Magmatic Province”. *Science*. 2011. 331(6023): 1404–1409.
416 10.1126/science.1199011.
- 417 27. M.F. Schaller, J.D. Wright, D.V. Kent, P.E. Olsen. “Rapid emplacement of the Central
418 Atlantic Magmatic Province as a net sink for CO_2 ”. *Earth and Planetary Science Letters*.
419 2012. 323–324: 27–39. 10.7916/D8PG22B4.
- 420 28. J.C. McElwain, D.J. Beerling, F.I. Woodward. “Fossil Plants and Global Warming at the
421 Triassic-Jurassic Boundary”. *Science*. 1999. 285(5432): 1386–1390.
422 10.1126/science.285.5432.1386.
- 423 29. T.E. Cerling. “Stable Carbon Isotopes in Palaeosol Carbonates”. *Palaeoweathering,*
424 *Palaeosurfaces and Related Continental Deposits*. Wiley-Blackwell, 2009. Pp. 43–60.

- 425 30. L.W. Diamond. "Review of the systematics of CO₂-H₂O fluid inclusions". *Lithos*. 2001.
426 55(1-4): 69-99. 10.1016/S0024-4937(00)00039-6.
- 427 31. J.L. Zimmermann, R. Moretto. "Release of water and gases from halite crystals". *European*
428 *Journal of Mineralogy*. 1996. 8(2): 413-422.
- 429 32. D.I. Norman, N. Blamey, J.N. Moore. "INTERPRETING GEOTHERMAL PROCESSES
430 AND FLUID SOURCES FROM FLUID INCLUSION ORGANIC COMPOUNDS AND
431 CO₂/N₂ RATIOS". Twenty-Seventh Workshop on Geothermal Reservoir Engineering.
432 2002.
- 433 33. A.E. Williams. "Mass spectrometric analysis of volatiles in fluid inclusions: aliquot
434 calibration valve to simulate inclusion rupture". *Chemical Geology*. 1996. 131(1): 155-165.
435 10.1016/0009-2541(96)00064-2.
- 436 34. M. Fries, A. Steele. "Raman Spectroscopy and Confocal Raman Imaging in Mineralogy and
437 Petrography". Springer Series in Optical Sciences. 2011. Pp. 111-135. 10.1007/978-3-642-
438 12522-5_6.
- 439 35. J.N. Butler. *Carbon Dioxide Equilibria and their Applications*. Routledge, New York, 1982.
440 10.1201/9781315138770.
- 441 36. T. Hrstka, J. Dubessy, J. Zachariáš. "Bicarbonate-rich fluid inclusions and hydrogen diffusion
442 in quartz from the Libčice orogenic gold deposit, Bohemian Massif". *Chemical Geology*.
443 2011. 281(3-4): 317-332. 10.1016/j.chemgeo.2010.12.018.
- 444 37. S. Facq, I. Daniel, G. Montagnac, H. Cardon, D.A. Sverjensky. "In situ Raman study and
445 thermodynamic model of aqueous carbonate speciation in equilibrium with aragonite under
446 subduction zone conditions". *Geochimica et Cosmochimica Acta*. 2014. 132: 375-390.
447 10.1016/j.gca.2014.01.030.
- 448 38. B.G. Oliver, A.R. Davis. "Vibrational Spectroscopic Studies of Aqueous Alkali Metal
449 Bicarbonate and Carbonate Solutions". *Can. J. Chem.* 1973. 51(5): 698-702. 10.1139/v73-
450 106.
- 451 39. W.W. Rudolph, D. Fischer, G. Irmer. "Vibrational Spectroscopic Studies and Density
452 Functional Theory Calculations of Speciation in the CO₂—Water System". *Appl Spectrosc.*
453 2006. 60(2): 130-144. 10.1366/000370206776023421.
- 454 40. W.W. Rudolph, G. Irmer, E. Königsberger. "Speciation studies in aqueous HCO₃⁻-CO₃²⁻-
455 solutions. A combined Raman spectroscopic and thermodynamic study". *Dalton Trans. The*
456 *Royal Society of Chemistry*, 2008. (7): 900-908. 10.1039/B713254A.
- 457 41. M.-C. Caumon, A. Tarantola, R. Mosser-Ruck. "Raman spectra of water in fluid inclusions:
458 I. Effect of host mineral birefringence on salinity measurement". *Journal of Raman*
459 *Spectroscopy*. 2015. 46(10): 969-976. 10.1002/jrs.4708.
- 460 42. J.D. Frantz. "Raman spectra of potassium carbonate and bicarbonate aqueous fluids at
461 elevated temperatures and pressures: comparison with theoretical simulations". *Chemical*
462 *Geology*. 1998. 152(3): 211-225.
- 463 43. J. Wu, H. Zheng. "Quantitative measurement of the concentration of sodium carbonate in the
464 system of Na₂CO₃-H₂O by Raman spectroscopy". *Chemical Geology*. 2010. 273(3): 267-
465 271. 10.1016/j.chemgeo.2010.03.001.

- 466 44. W.W. Rudolph, G. Irmer, E. Königsberger. “Speciation studies in aqueous HCO₃⁻—CO₃²⁻
467 solutions. A combined Raman spectroscopic and thermodynamic study”. Dalton Trans. The
468 Royal Society of Chemistry, 2008. (7): 900–908. 10.1039/B713254A.
- 469 45. Q. Sun, C. Qin. “Raman OH stretching band of water as an internal standard to determine
470 carbonate concentrations”. Chemical Geology. 2011. 283(3): 274–278.
471 10.1016/j.chemgeo.2011.01.025.
- 472 46. K.E. Chave. “Evidence on History of Sea Water from Chemistry of Deeper Subsurface
473 Waters of Ancient Basins¹”. AAPG Bulletin. 1960. 44(3): 357–370. 10.1306/0BDA5FF3-
474 16BD-11D7-8645000102C1865D.
- 475 47. F.T. Mackenzie, R.M. Garrels. “Chemical mass balance between rivers and oceans”.
476 American Journal of Science. American Journal of Science, 1966. 264(7): 507–525.
477 10.2475/ajs.264.7.507.
- 478 48. R.M. Garrels, F. Mackenzie. “Origin of the Chemical Compositions of Some Springs and
479 Lakes”. Am. Chem. Soc. Adv. Chem. Ser. 1967. Pp. 222–242. 10.1021/ba-1967-0067.ch010.
- 480 49. S.D. Burley, J. Mullis, A. Matter. “Timing diagenesis in the Tartan Reservoir (UK North
481 Sea): constraints from combined cathodoluminescence microscopy and fluid inclusion
482 studies”. Marine and Petroleum Geology. 1989. 6(2): 98–120. 10.1016/0264-
483 8172(89)90014-7.
- 484 50. W. Stumm, J.J. Morgan. Aquatic Chemistry: Chemical Equilibria and Rates in Natural
485 Waters. Wiley, 1996.
- 486 51. D. Langmuir. Aqueous Environmental Geochemistry. 1st edition. Prentice Hall, Upper
487 Saddle River, N.J, 1997.
- 488 52. M.E. Sumner, ed. Handbook of Soil Science. 1st edition. CRC Press, Boca Raton, Fla, 1999.
- 489 53. F.J. Millero, T.B. Graham, F. Huang, H. Bustos-Serrano, D. Pierrot. “Dissociation constants
490 of carbonic acid in seawater as a function of salinity and temperature”. Marine Chemistry.
491 2006. 100(1): 80–94. 10.1016/j.marchem.2005.12.001.
- 492 54. K. Onda, E. Sada, T. Kobayashi, S. Kito, K. Ito. “SALTING-OUT PARAMETERS OF GAS
493 SOLUBILITY IN AQUEOUS SALT SOLUTIONS”. J. Chem. Eng. Japan / JCEJ. 1970.
494 3(1): 18–24. 10.1252/jcej.3.18.
- 495 55. J.N. Butler. Ionic Equilibrium: Solubility and pH Calculations. John Wiley & Sons, 1998.
- 496 56. J.I. Drever. The Geochemistry of Natural Waters: Surface and Groundwater Environments.
497 Prentice Hall, 1997.
- 498 57. T. Dieing, O. Hollricher. “High-resolution, high-speed confocal Raman imaging”.
499 Vibrational Spectroscopy. 2008. 48(1): 22–27. 10.1016/j.vibspec.2008.03.004.
- 500 58. A.R. Davis, B.G. Oliver. “A Vibrational-Spectroscopic Study of the Species Present in the
501 CO₂-H₂O System”. Journal of Solution Chemistry. 1972. 1(4): 11.
- 502 59. J.D. Pasteris, O. Beyssac. “Welcome to Raman Spectroscopy: Successes, Challenges, and
503 Pitfalls”. Elements. 2020. 16(2): 87–92. 10.2138/gselements.16.2.87.

- 504 60. G. Giridhar, R.R.K.N. Manepalli, G. Apparao. “Confocal Raman Spectroscopy”.
505 Spectroscopic Methods for Nanomaterials Characterization. Elsevier, 2017. Pp. 141–161.
506 10.1016/B978-0-323-46140-5.00007-8.
- 507 61. R.H. Goldstein. Chapter 2: Petrographic Analysis of Fluid Inclusions. Mineral. Assoc.
508 Canada, 2003.
- 509 62. K.M. Rosso, R.J. Bodnar. “Microthermometric and Raman spectroscopic detection limits of
510 CO₂ in fluid inclusions and the Raman spectroscopic characterization of CO₂”. *Geochimica
511 et Cosmochimica Acta*. 1995. 59(19): 3961–3975. 10.1016/0016-7037(95)94441-H.
- 512 63. Y. Kawakami, J. Yamamoto, H. Kagi. “Micro-Raman Densimeter for CO₂ Inclusions in
513 Mantle-Derived Minerals”. *Appl Spectrosc.* 2003. 57(11): 1333–1339.
514 10.1366/000370203322554473.
- 515 64. X. Wang, W. Hu, I.-M. Chou. “Raman spectroscopic characterization on the OH stretching
516 bands in NaCl–Na₂CO₃–Na₂SO₄–CO₂–H₂O systems: Implications for the measurement of
517 chloride concentrations in fluid inclusions”. *Journal of Geochemical Exploration*. 2013. 132:
518 111–119. 10.1016/j.gexplo.2013.06.006.
- 519 65. J.J. Carroll, J.D. Slupsky, A.E. Mather. “The Solubility of Carbon Dioxide in Water at Low
520 Pressure”. *Journal of Physical and Chemical Reference Data*. American Institute of Physics,
521 1991. 20(6): 1201–1209. 10.1063/1.555900.
- 522 66. R. Wiebe, V.L. Gaddy. “The Solubility of Carbon Dioxide in Water at Various Temperatures
523 from 12 to 40° and at Pressures to 500 Atmospheres. Critical Phenomena *”. *J. Am. Chem.
524 Soc.* 1940. 62(4): 815–817. 10.1021/ja01861a033.
- 525 67. R.E. Zeebe, D. Wolf-Gladrow. CO₂ in Seawater: Equilibrium, Kinetics, Isotopes. Gulf
526 Professional Publishing, 2001.
- 527 68. M.J. Pelletier. *Analytical Applications of Raman Spectroscopy*. 1st edition. Blackwell
528 Publishing, Osney Mead, Oxford ; Malden, MA, 1999.
- 529 69. J.A. Hurowitz, D.C. Catling, W.W. Fischer. “High Carbonate Alkalinity Lakes on Mars and
530 their Potential Role in an Origin of Life Beyond Earth”. *Elements*. 2023. 19(1): 37–44.
531 10.2138/gselements.19.1.37.
- 532

Figures and Tables

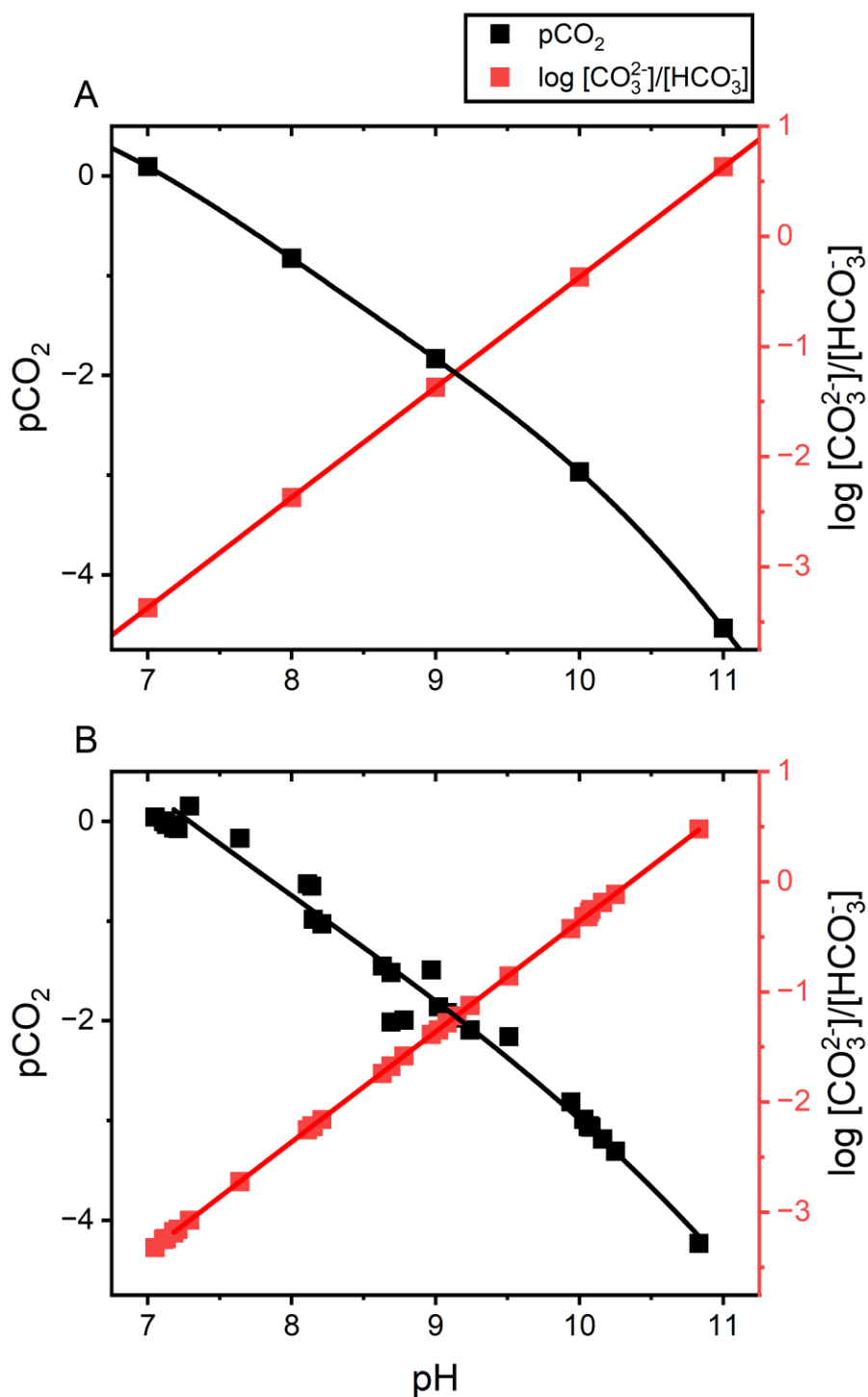


Figure 1. (A) Theoretical calculations of the relationship between the ratio of [CO₃²⁻] and [HCO₃⁻], pH, and pCO₂. The theoretical relationship can be used to estimate pCO₂ over a wide range of alkaline solutions. (B) Solutions used in this study shows the relationship between the ratio of [CO₃²⁻] and [HCO₃⁻], and pH can calibrate for a wide range of pCO₂.

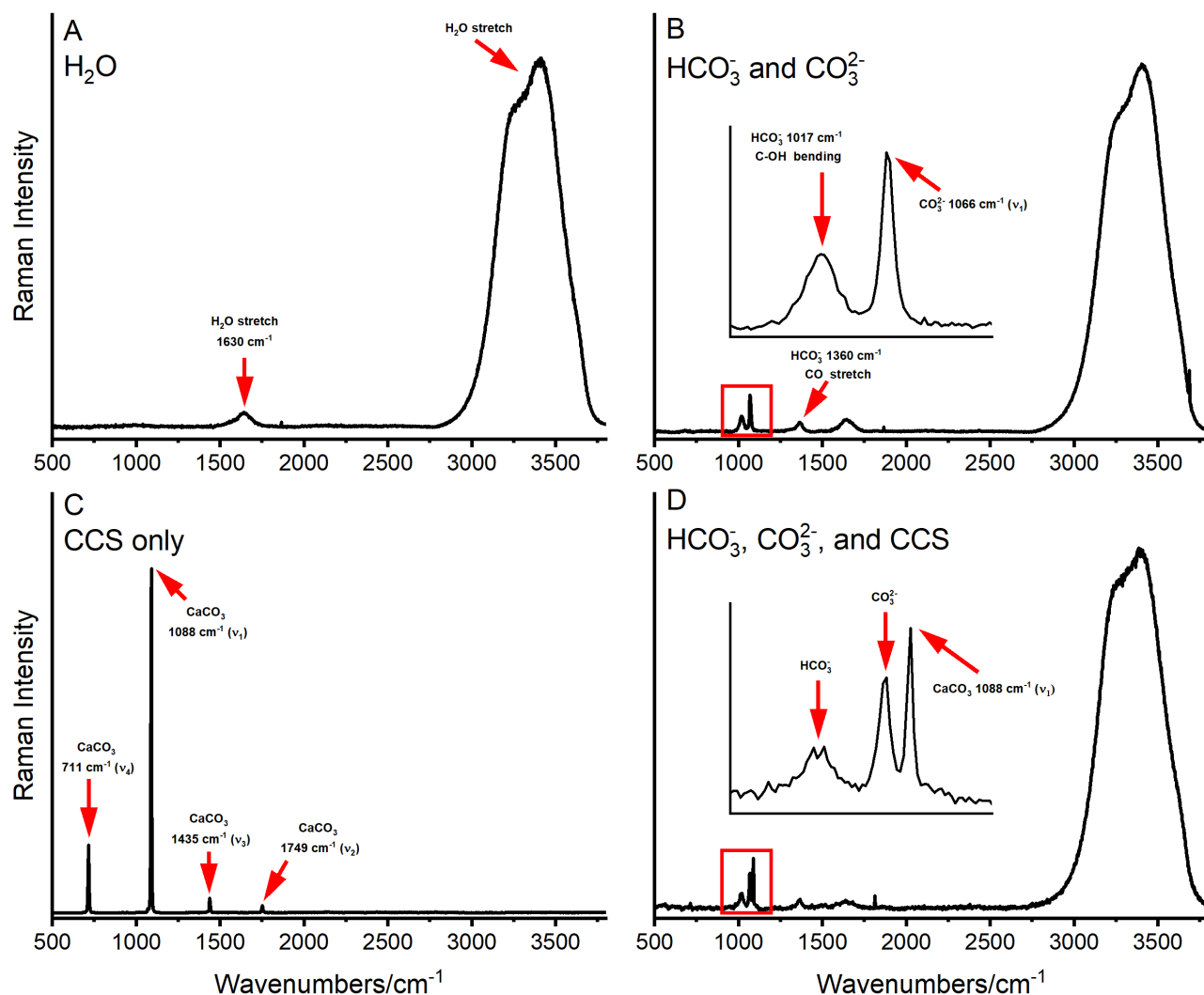


Figure 2. Background corrected Raman spectra of the different components used to build the calibration curves. A) Raman spectra of the Millipore water used to make the solutions. B) Raman spectra of a 0.15 molar NaHCO₃ and 0.03 molar Na₂CO₃ solution with inset of the red box in an area between 950 – 1150 cm⁻¹. The main HCO₃⁻ and CO₃²⁻ band is at ~1017 and ~1066 cm⁻¹, respectively. C) Raman spectra of the calcite cover slip (CCS) with the main CaCO₃ peak at ~1088 cm⁻¹. D) Raman spectra of the 0.15 molar NaHCO₃ and 0.03 molar Na₂CO₃ solution with the Raman focused 100 μm below the calcite cover slip with an inset that shows the respective positions of the HCO₃⁻, CO₃²⁻, and CaCO₃ peaks. Abbreviations: T, translational lattice; v₁, symmetric stretching vibration; v₂, out-of-plane bending vibration; v₃, antisymmetric stretching vibration; v₄, in-plane bending vibration.

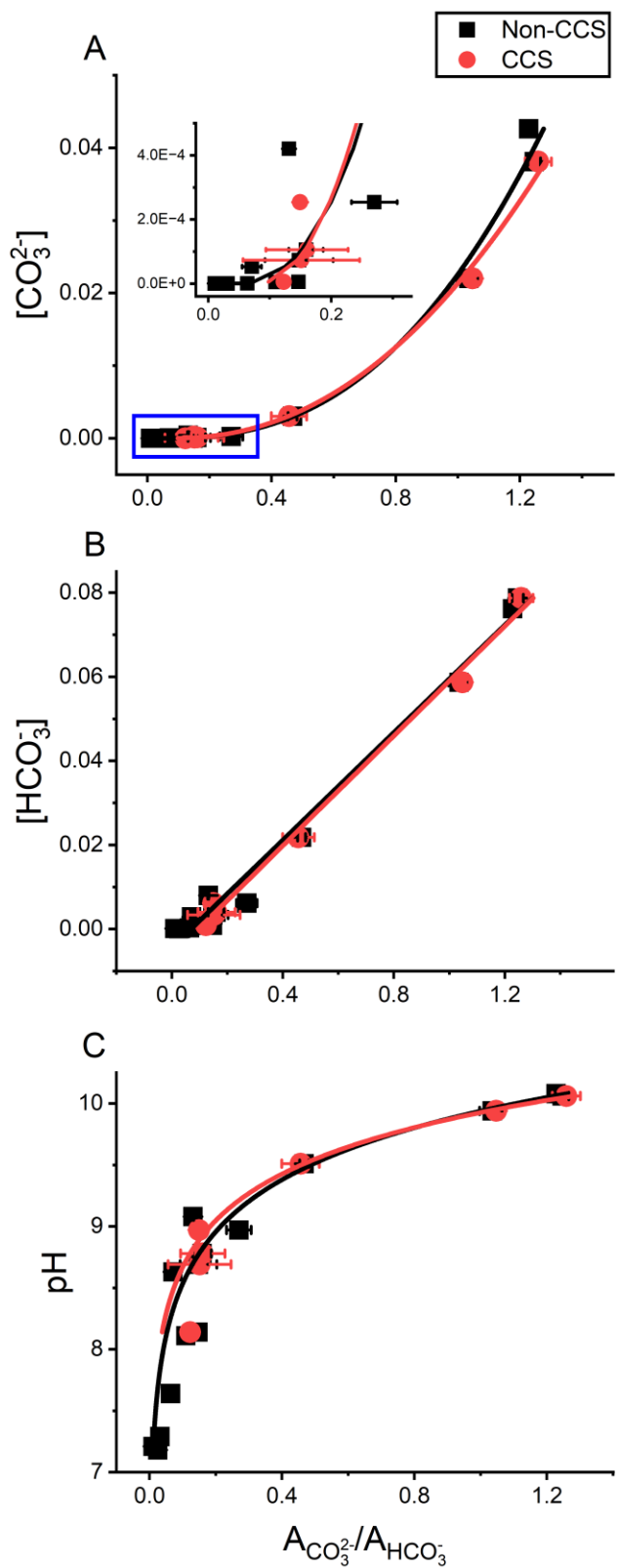


Figure 3. Comparisons of carbonate species concentrations and pH solution calibrations with (red) and without (black) the calcite cover slip (CCS). Solution calibrations of $[\text{CO}_3^{2-}]$ (A), $[\text{HCO}_3^-]$ (B), and pH (C) versus the area ratio between CO_3^{2-} and HCO_3^- peaks. Blue box represents the inset within (A). Concentrations are in mol/L.

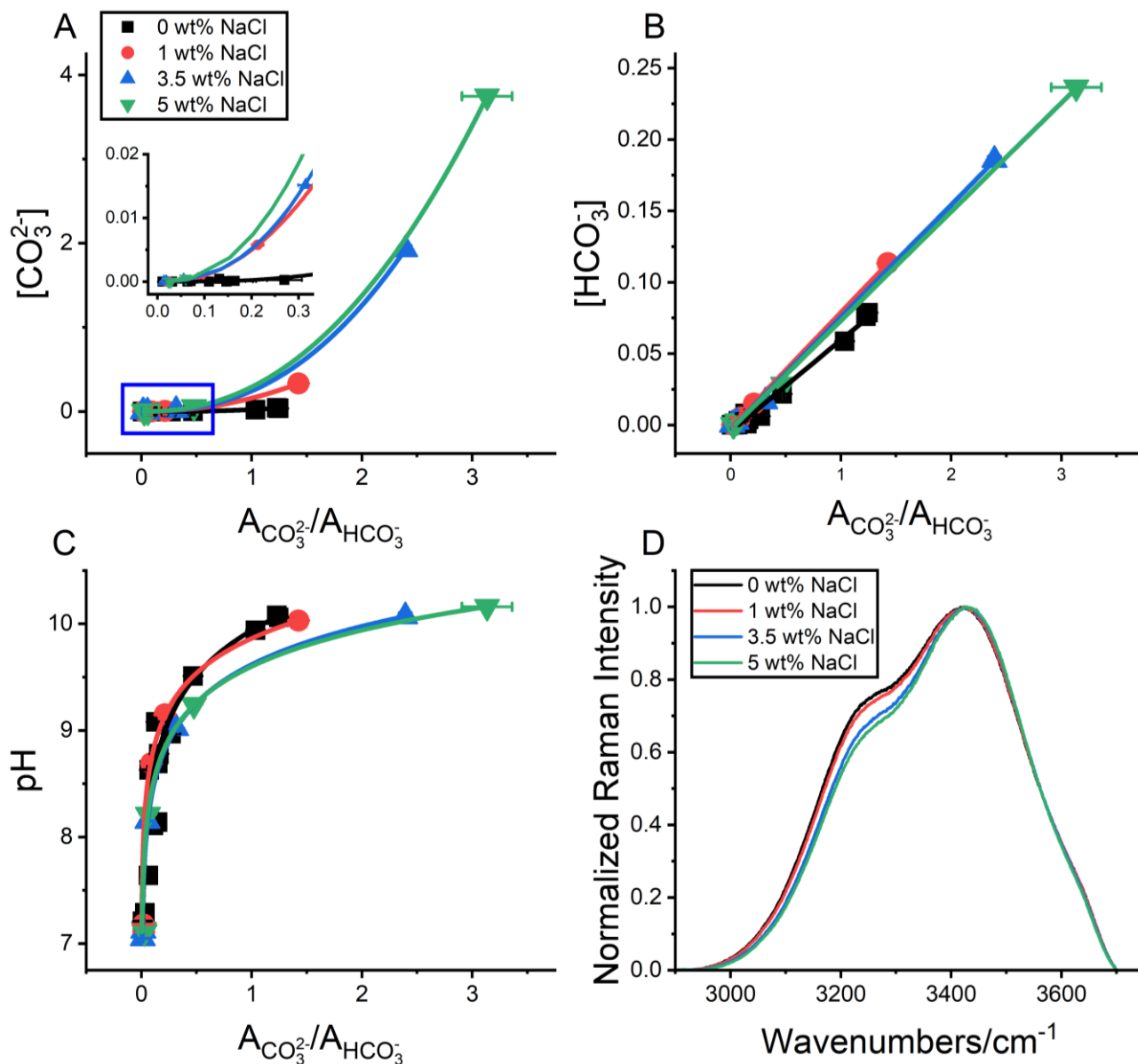


Figure 4. Comparisons of carbonate species concentrations (CO_3^{2-} and HCO_3^-) and pH solution calibrations at various NaCl concentrations (salinities). Solution calibrations of $[\text{CO}_3^{2-}]$ (A), $[\text{HCO}_3^-]$ (B), and pH (C) versus area ratios between the CO_3^{2-} and HCO_3^- peaks. Normalized Raman OH⁻ stretch at different NaCl concentrations. Blue box represents the inset within (A). Concentrations are in mol/L.

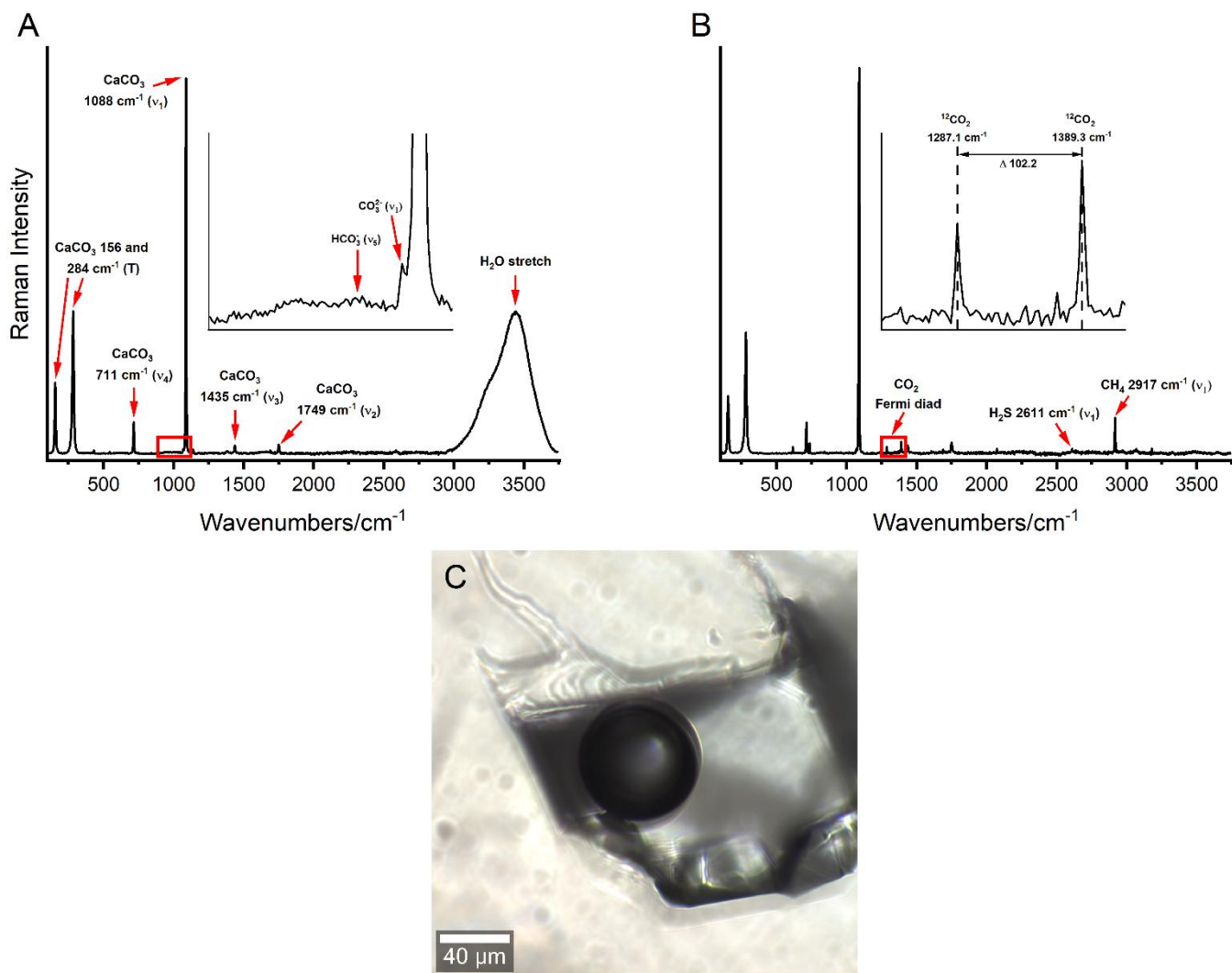


Figure 5. Example Raman spectra of the liquid (A) and gas phase (B) of the large fluid inclusion measured in this study. Liquid phase showing HCO_3^- (1017 cm^{-1}), CO_3^{2-} (1066 cm^{-1}), and H_2O (1630 and $2750\text{-}3750 \text{ cm}^{-1}$) peaks with an inset of the red box for the HCO_3^- and CO_3^{2-} peaks. Gas phase shows the CO_2 Fermi diad (1285 and 1388 cm^{-1}), hydrogen sulfide (2611 cm^{-1}), and methane (2917 cm^{-1}). Gas phase inset of the red box shows the CO_2 Fermi diad and the difference between peak distance (Δ) estimates fluid density. Host mineral calcite peaks are present in both in liquid and gas phase spectra at (156 , 284 , 711 , 1088 , and 1435 cm^{-1}). Photomicrograph of the analyzed fluid inclusion in Iceland Spar (C). Abbreviations: T, translational lattice; ν_1 , symmetric stretching vibration; ν_2 , out-of-plane bending vibration; ν_3 , antisymmetric stretching vibration; ν_4 , in-plane bending vibration.

Environment	[CO ₃ ²⁻]	[HCO ₃ ⁻]	pH	Reference
Oceans	0.0002 - 0.0003	0.002 - 0.03	7.4 - 8.3	35,46-48
Rivers	3.6x10 ⁻⁸	0.0005 - 0.002	5.28 - 8.5	35,47,50,69
Groundwater	0.00169	0.0001 - 0.003	5.1 – 10.7	51,52,69
Soil	-	0.0001 - 0.003	4.8 - 10.02	51,52
Fluid Inclusions	-	0.007 - 0.014	-	49

Table 1. Range of carbonate and bicarbonate concentrations (mol/L), and pH in natural waters.

NaCl wt%	pH	[CO ₃ ²⁻]	[HCO ₃ ⁻]	ACO ₃ ²⁻ /AHCO ₃ ⁻ (non-CCS)	ACO ₃ ²⁻ /AHCO ₃ ⁻ (CCS)
0	10.08	0.0426	0.0762	1.228	-
0	10.06	0.0381	0.0787	1.246	1.259
0	9.94	0.0220	0.0587	1.035	1.047
0	9.51	0.0030	0.0218	0.467	0.456
0	9.08	4.2E-04	0.0080	0.131	-
0	8.97	2.5E-04	0.0062	0.270	0.149
0	8.78	1.1E-04	0.0040	0.159	0.160
0	8.69	7.3E-05	0.0034	0.147	0.151
0	8.63	5.3E-05	0.0029	0.071	-
0	8.14	5.6E-06	0.0009	0.146	0.123
0	8.11	4.8E-06	0.0009	0.110	-
0	7.64	5.5E-07	0.0003	0.063	-
0	7.29	1.1E-07	1.3E-04	0.031	-
0	7.21	7.6E-08	1.1E-04	0.010	-
0	7.18	6.7E-08	1.0E-04	0.025	-
1	10.03	0.3326	0.1133	1.425	-
1	9.15	0.0058	0.0149	0.213	-
1	8.69	0.0007	0.0052	0.090	-
1	7.18	6.6E-07	1.6E-04	0.019	-
1	7.11	4.8E-07	1.4E-04	0.022	-
3.5	10.07	1.927	0.1856	2.393	-
3.5	9.02	0.0152	0.0165	0.315	-
3.5	8.15	2.8E-04	2.2E-03	0.055	-
3.5	7.12	2.4E-06	2.1E-04	0.018	-
3.5	7.05	1.7E-06	1.8E-04	0.013	-
5	10.16	3.7454	0.2365	3.134	-
5	9.24	0.0538	0.0284	0.477	-
5	8.21	4.8E-04	0.0027	0.060	-
5	7.13	3.2E-06	2.2E-04	0.023	-
5	7.11	2.9E-06	2.1E-04	0.028	-

Table 2. Solutions and associated area ratio of carbonate species to water, with and without the calcite cover slip (CCS), measured using Confocal Raman spectroscopy.

	Test	Equation	R ²	95% CI
Non-CCS	[CO ₃ ²⁻]	$y = 0.021x^{3.12}$	0.99	0.018-0.023
	[HCO ₃ ⁻]	$y = 0.064x - 0.004$	0.99	0.059-0.069
	pH	$y = \frac{\ln(\frac{x}{8.44 \cdot 10^{-8}})}{1.64}$	0.99	1.42-1.86
CCS	[CO ₃ ²⁻]	$y = 0.020x^{2.83}$	0.99	0.019-0.021
	[HCO ₃ ⁻]	$y = 0.065x - 0.006$	0.99	0.060-0.070
	pH	$y = \frac{\ln(\frac{x}{1.28 \cdot 10^{-8}})}{1.83}$	0.99	1.48-2.18

Table 3. Results of [CO₃²⁻], [HCO₃⁻], and pH estimation correlations with and without the calcite cover slip (CCS).

Test	NaCl wt%	Equation	R ²	95% CI
[CO ₃ ²⁻]	1 wt%	$y = 0.16x^{2.14}$	0.99	0.15-0.16
	3.5 wt%	$y = 0.24x^{2.39}$	0.99	0.24-0.24
	5 wt%	$y = 0.24x^{2.39}$	0.99	0.24-0.24
[HCO ₃ ⁻]	1 wt%	$y = 0.081x - 0.002$	0.99	0.08-0.082
	3.5 wt%	$y = 0.079x - 0.003$	0.99	0.073-0.084
	5 wt%	$y = 0.077x - 0.004$	0.99	0.073-0.080
pH	1 wt%	$y = \frac{\ln\left(\frac{x}{7.80 * 10^{-10}}\right)}{2.13}$	0.99	1.9-2.3
	3.5 wt%	$y = \frac{\ln\left(\frac{x}{8.26 * 10^{-9}}\right)}{1.93}$	0.99	1.9-2.0
	5 wt%	$y = \frac{\ln\left(\frac{x}{3.08 * 10^{-9}}\right)}{2.04}$	0.99	1.93-2.16

Table 4. Results of [CO₃²⁻], [HCO₃⁻], and pH estimation correlations at different NaCl wt%.

[CO ₃ ²⁻]	[HCO ₃ ⁻]	pH	pCO ₂	CO ₂ (ppm)
0.05 ± 0.08	0.04 ± 0.02	9.46 ± 0.31	-3.62 ± 0.19	240 ± 132

Table 5. Estimated CO₃²⁻ and HCO₃⁻ concentrations, pH, pCO₂, and CO₂ (ppm) of the calcite fluid inclusion.